J. Inst. Eng. India Ser. B
https://doi.org/10.1007/s40031-024-01056-5

ORIGINAL CONTRIBUTION

Wavelet Analysis and Machine Learning Approach for Improved Protection of PV-Wind-SVC Integrated Smart Power System

Gantaiah Swamy Garika[1] · **Padma Kottala**[2]

Received: 11 October 2023 / Accepted: 28 March 2024

Abstract In order to assure uninterrupted electrical power transmission throughout a nation's network, it is necessary to integrate reactive power compensation devices and renewable energy sources in addition to other systematic maintenance procedures to maintain balance and regulate voltage changes. A responsive security system is essential to guard against disturbances caused by both balanced and unbalanced electrical problems. By employing wavelet and machine learning analysis to analyze transitory signals using mathematical and electrical concepts, this work sheds light on power network problems. The growing use of reactive power devices and renewable energy sources, however, comes with difficulties because of demand fluctuations, uncertainty around renewable supply, and grid complexity that is exacerbated by unidentified grid models. The study uses supervised and unsupervised machine learning methods to address these issues and advance power system analysis. By using a wavelet-based machine learning approach, the suggested algorithm has been tested for the detection and discrimination of fault behavior in PV-Wind integrated power system networks in the presence and absence of Static Var compensator. It has been shown that the algorithm is more effective than traditional techniques.

Keywords Wind energy source · Solar-PV · SVC · Wavelet transform · Fault detection · Machine learning · Internet-of-Things (IoT)

Introduction

In order to link electrical devices and allow electricity to go from generation terminals to consumers, the power network is necessary. However, the network is vulnerable to electrical faults caused by adverse weather conditions, resulting in damage to power conductors and disruptions in power flow. To address this, a protective relaying scheme with a synchronizing mechanism is needed to isolate faulty equipment from the functioning network [1]. The existing protection scheme, known as distance protection, calculates impedance at relay points but has drawbacks such as tripping during normal conditions, temporary faults, power swings, and overloads [2]. Frequent false tripping can lead to system blackouts, necessitating alternative methods for safeguarding electrical components. A prospective scheme should provide fast fault detection and isolation of faulty equipment through a relay mechanism, aided by digital communication and global synchronization [3, 4]. Currently, power network security primarily focuses on electrical problems, but mechanical damage can also occur. To ensure comprehensive protection, the monitoring of connected devices should cover both electrical and mechanical aspects. IoT devices can be utilized alongside electrical measurements to monitor the power distribution system for issues such as voltage fluctuations, power loss, and power imbalance. The installation of shunt/series compensating devices can help mitigate these complications. The protection scheme should address faults in the main and microgrid, considering different current flow directions and magnitudes [5]. Modern compensating devices, employing

✉ Gantaiah Swamy Garika
swamyaliet@gmail.com

Padma Kottala
dr.kpadma@andhrauniveristy.edu.in

[1] Department of Electrical and Electronics Engineering, Andhra Loyola Institute of Engineering and Technology, Vijayawada 520013, India

[2] Electrical Engineering, Andhra University College of Engineering, Visakhapatnam 530003, India

Published online: 22 April 2024

power electronics switching devices, require special protection schemes. A static Var Compensator (SVC) made up of TCR,TSC,FC and a mix of photovoltaic and wind energy sources is the test system that has been proposed [6, 7]. However, the presence of FACTS devices, particularly in SVC connected systems, introduces challenges related to under-reach phenomena [8]. Wavelet detailed coefficients are used for fault detection and discrimination, while artificial neural networks (ANNs) are employed to locate faults in the power network based on current measurements [9, 10]. Power systems are complex and immense, requiring efficient decision-making methods for operation and control tasks. With the integration of renewable energy sources and evolving demand patterns, power grid operations have undergone significant transformations. To address the resulting complications and unknown models, supervised and unsupervised machine learning algorithms [11] have been rapidly adopted for predicting the stability of different types and sizes of power systems during sudden changes using a specialized machine learning technique called twin convolution support vector machine (TCSVM) [12]. This method involves collecting and processing power system data, creating a model that combines aspects of image analysis and classification, training and validating the model, and potentially applying it to real-world power systems to predict stability outcomes. The ultimate goal is to develop a versatile and accurate tool for power system engineers to assess transient stability [13, 14].

The conventional algorithms used previously took a considerable amount of time, approximately 2 cycles, to identify and differentiate faults. Additionally, there was a deficiency in physically monitoring system performance. The proposed research emphasizes IoT monitoring of solar energy, wind energy, and reactive power compensated devices within a wide-area power network, achieving a security level of less than half a cycle time using Multi-Resolution Analysis (MRA) with wavelet coefficients derived from the Bior-1.5 mother wavelet. This study seeks to improve the digital relays' interaction with the power network, facilitating quicker isolation of faulty equipment compared to traditional methods.

Mathematical modeling and System Analysis

The wind farms and PV-Solar sources are natural and sustainable energy resources that generate electricity through the transformation of solar and wind energy. In the test power network, a Static Var Compensator (SVC) is incorporated for reactive power compensation, along with Photo-Voltaic (PV) and wind energy sources. The mathematical modeling of these devices is described as follows:

Photovoltaic(PV)Solar Source

The investigation on how high-voltage power transmission lines affect photovoltaic energy output might have the effects of high-voltage power transmission lines on photovoltaic (PV) power generating systems' output and efficiency. As solar energy becomes a prominent renewable source, understanding the interaction between PV panels and nearby transmission lines is crucial for efficient energy integration. We analyze the effects of electromagnetic interference, shadowing, noise, and vibrations caused by transmission lines on PV systems. The extent to which these factors impact PV panel performance and overall energy production. Additionally, we explore potential mitigation strategies to minimize these adverse effects and enhance the reliability of solar energy integration. The findings of this study contribute to informed urban planning, solar farm design, and sustainable energy policy decisions. The insights gained hold significance for both optimizing renewable energy systems and ensuring the seamless integration of solar power into existing grids [15, 16].

The mathematical modeling of a solar photovoltaic (PV) system involves describing the electrical behavior of the PV module and its relationship with solar irradiance and temperature conditions. Overall, the mathematical model of a solar photovoltaic system combines the electrical behavior of the PV module, the influence of solar irradiance, and the temperature dependence to predict the power output under different operating conditions. These models are essential for system design, performance evaluation, and optimization of solar PV systems.

A mathematical model of a solar photovoltaic (PV) system describes the relationship between various parameters and components involved in the generation of electricity from sunlight. The model typically takes into account factors such as solar irradiance, temperature, efficiency of the PV cells, and other system-specific parameters. Here's a simplified example of a mathematical model for a solar PV system:

Solar Irradiance (G): the amount of solar energy received per unit area, usually measured in watts per square meter(W/m2).

Temperature (T): the operating temperature of the PV cells. Higher temperatures can reduce the efficiency of the cells.

PV Cell Efficiency (η): the efficiency of converting sunlight into electricity, expressed as the ratio of electrical power output to solar energy input.

PV Array Area (A): the total area covered by the PV modules.

Electrical Power Output (Pout): the actual electrical power produced by the PV system.

When it comes to the mathematical modeling of a solar photovoltaic (PV) system, it includes the representation of the

PV module's electrical behavior and how it relates to temperature and solar ir- radiance. A solar photovoltaic system's mathematical model combines the PV module's electrical properties, the effect of sun irradiation, and temperature dependency to predict power output under various operating scenarios involved in producing energy from sunshine. Commonly, this model takes into account variables like temperature, solar irradiation, PV cell efficiency, and other system-specific characteristics. An illustration of such a mathematical model for a photovoltaic system may be found here:

The mathematical model can be represented as:

$$P_{\text{out}} = GXAX\eta Xf(T)$$

where Pout is the electrical power output of the PV system. G is the solar irradiance. A is the PV array area. η is the PV cell efficiency. $f(T)$ is a function that considers the temperature effect on efficiency. The function $f(T)$ could be a simple linear or nonlinear relationship that considers the temperature coefficient of the PV cells. Generally, as temperature increases, efficiency decreases. A few essential formulas for modeling solar photovoltaic (PV) systems. Remember that these are simplified versions of the equations; real-world models might have more intricate variables and parameters. Here is a summary of a few key equations: Equation for the characteristic of current–voltage (*I–V*): The behavior of a PV cell or module under various operating conditions is described by the *I–V* characteristic equation. Frequently employed is the Shockley diode equation:

$$I = I_{\text{ph}} - I_{\text{sat}}\left(\exp\left(\frac{V + I \cdot R_{\text{ser}}}{a \cdot V_{\text{th}}}\right) - 1\right) \tag{1}$$

where I, I_{ph}, I_{sat} is the cell/module current, photo current(current generated by light),reverse saturation current. V is the voltage across the cell/module terminals. R_{ser} is the series resistance. a is the diode ideality factor. V_{th} is the thermal voltage (kT/q, where k is Boltzmann's constant, T is temperature, and q is the elementary charge).

P–V Characteristic Equation: the power–voltage (*P–V*) characteristic of a *PV* cell/module provides insights into its power generation capabilities:

$$P = I \cdot V \tag{2}$$

where P is the power output of the cell/module.

Single-Diode Model: this is an extended version of the *I–V* characteristic equation that includes parameters like shunt resistance (R_{sh}) and considers the non-ideal behavior of the *PV* cell/module:

$$I = I_{\text{ph}} - I_{\text{sat}}\left(\exp\left(\frac{V + I \cdot R_{\text{ser}}}{a \cdot V_{\text{th}}}\right) - 1\right) - \frac{V + I \cdot R_{\text{ser}}}{R_{\text{sh}}} \tag{3}$$

Temperature Effects: the *PV* cell/module efficiency and performance are influenced by temperature. The temperature adjusted *I–V* equation considers this effect:

$$I = I_1 + I_2 \tag{4}$$

$$I_1 = I_{\text{ph}} - I_{\text{sat}}\left(\exp\left(\frac{V + I \cdot \left(R_{\text{ser}} + R_{temp}.\Delta T\right)}{a \cdot V_{\text{th}}}\right) - 1\right) \tag{5}$$

$$I_2 = -\left(\frac{V + I \cdot \left(R_{\text{ser}} + R_{temp}.\Delta T\right)}{R_{sh}}\right) \tag{6}$$

This equation describes the current–voltage (*I–V*) relationship of a photovoltaic cell/module, accounting for temperature effects. It includes terms for photocurrent (I_{ph}), reverse saturation current (I_{sat}), voltage (V), series resistance (R_{ser}), temperature-dependent series resistance (R_{temp}), diode ideality factor (a), thermal voltage (V_{th}), temperature difference (ΔT), and shunt resistance (R_{sh}). Where ΔT is the temperature difference from the reference temperature.

System-Level Equations: to model a complete solar *PV* system, you'd integrate the cell/module models into a system- level model that includes factors like shading, inverter efficiency, and electrical losses. The system's overall power output can be estimated as the total of each cell's or module's individual power outputs:

$$P_{\text{out,system}} = \sum_{i=1}^{n} P_{\text{out,cell}} \tag{7}$$

These equations provide a foundation for modeling solar *PV* systems. Keep in mind that real-world modeling can involve additional complexities and factors, and specialized software tools are often used for accurate system simulations (Figs. 1, 2, 3).

The following is a description of the photovoltaic (*PV*) array's mathematical equivalent circuit: the solar irradiance (I_r), (I_{sc}) and (k_i) short-circuit current and constant, and operating temperature (T) in Kelvin are used

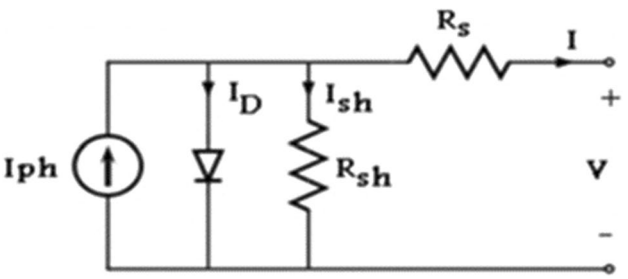

Fig. 1 CircuitequaltoaPVcell

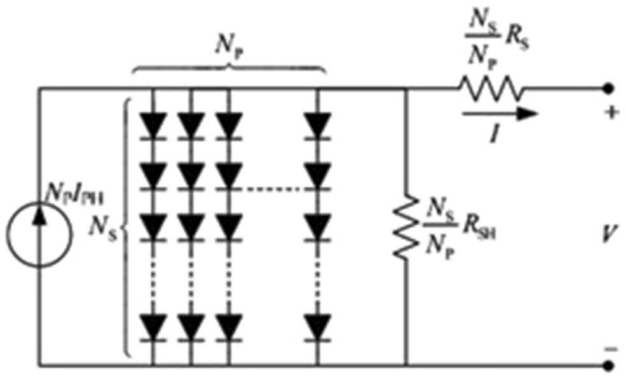

Fig. 2 The PVequivalentcircuit-Array

to calculate the photo current (I_{ph}) of the *PV* cell. This formula is used to calculate it.

$$I_{ph} = \frac{\left[k_i(T - 298) + Isc\right] \times I_r}{1000} \tag{8}$$

The module saturation current (I_0) is computed using the Richardson-Dushman equation. It depends on the reverse saturation current of the cell (I_{rs}), the Boltzmann constant (k), the ideality factor (n), the temperature (T), and the band gap energy (E_{g0}). The formula for $I_0$is given by

$$I_0 = I_{rs}\left[\frac{T}{I_r}\right]^3 \exp\left[\frac{q \times E_{g0}}{nk}\left(\frac{1}{T} - \frac{1}{T_r}\right)\right] \tag{9}$$

where *Tr* is the reference temperature (298.15 K) and Eg0is the band gap energy (1.1 eV).

The thermal voltage (V_t) is determined during the Boltzmann constant (k) and the absolute temperature (T) in Kelvin:

$$V_t = \frac{k \times T}{q} \tag{10}$$

The shunt current (I_{sh}) represents the current flowing through the shunt resistance (R_{sh}).It is computed based on the voltage across the shunt resistance (V) and the number of modules in parallel (N_p) and series (N_s), as well as the series resistance (R_s). The formula for I_{sh} is given by:

$$I_{\text{sh}} = \frac{V \times \frac{N_p}{N_s} + 1 \times R_s}{R_{\text{sh}}} \tag{11}$$

Solar energy modules may instantly transform radiant solar energy into low voltage, which is then increased to the required voltage level using DC–DC converters and switch-mode regulators. For a variety of grid connections and applications, this regulated DC output voltage is suitable.

Wind Energy Conversion System modeling

The wind energy source captures the kinetic energy from moving air to produce electrical power. Its mathematical representation incorporates various characteristics of the wind turbine, encompassing the power coefficient, wind velocity, and turbine parameters. This model takes into account factors like wind direction, fluctuations in wind speed, and the efficiency of the turbine to compute the resulting power output.

Wind energy is transformed into electrical energy during the process, producing a low alternating current (AC) voltage output. A mix of buck and boost converters is used to raise this AC voltage output to an appropriate transmission level [17]. The Doubly-Fed Induction Generator (DFIG) wind turbine, which is the centerpiece of the proposed system, is made up of necessary parts. These DFIG turbines, which are commonly used, generate electricity by using coupled turbines and generators to capture the kinetic energy of the wind [18]. The generator has windings on its rotor and stator that can send electricity to the utility grid.

The generator boasts distinctive features, including a grid-connected stator and a bidirectional power converter integrated into the rotor, as depicted in Fig. 4. These components consist of two IGBT bridge voltage-source converters linked to a DC connection. This configuration enables the system to dynamically adjust its frequency. The following equations elucidate

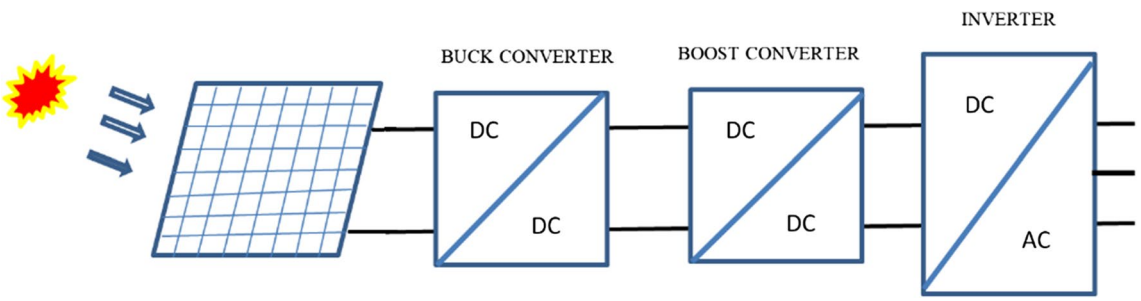

Fig. 3 Solar PV model representation

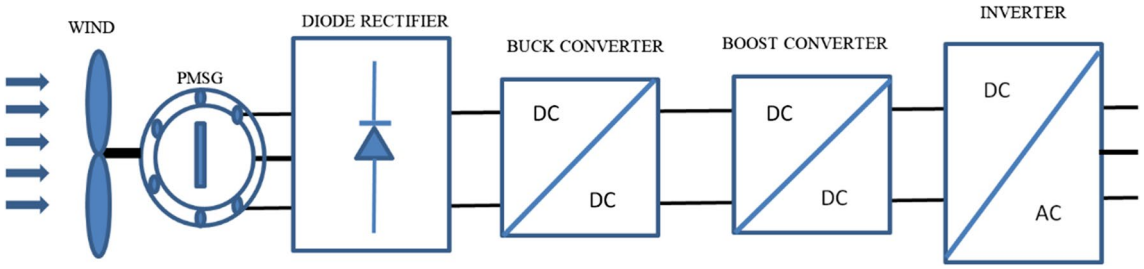

Fig. 4 Model for producing energy from windmill

how modulation of the turbine rotor's blade angle governs the strength and rotational speed of powerful winds.

The development of the mathematical model for the Doubly-Fed Induction Generator (DFIG) relies on the application of fundamental principles from the domains of electrical and mechanical systems. These principles are leveraged to elucidate the dynamic behavior of the DFIG. Specifically, the derivation of the DFIG model equations is rooted in the principles of electromagnetism and rotational mechanics.

As seen in Fig. 4, the generator has unique characteristics such as a bidirectional power converter built into the rotor and a stator connected to the grid. Two IGBT bridge voltage-source converters connected to a DC connector make up these parts. With this setup, the system can dynamically change its frequency. The strength and rotational speed of strong winds are controlled by varying the blade angle of the turbine rotor, as shown by the following formulae.

Representing the parts and interactions of a wind turbine system is necessary when developing a mathematical model for a Wind Energy Conversion System (WECS). An overview of the essential elements and formulas used frequently in wind energy system modeling is provided below.

$$P_{\text{turbine}}(\vartheta) = \left\{ \begin{array}{c} 0, \vartheta < \vartheta_{\text{cut-in}} \\ 0, \vartheta > \vartheta_{\text{cut-out}} \\ \frac{1}{2}\rho.\Delta.C_p(\vartheta).\vartheta^3 \\ P_{\text{rated}}, \vartheta_{\text{rated}} \geq \vartheta \geq \vartheta_{\text{cut-out}} \end{array} \right\} \quad (12)$$

where v is the wind speed. ρ is the air density. A is the swept area of the rotor. $C_p(v)$ is the power coefficient at a given wind speed. Prated is the rated power of the turbine. $v_{\text{cut-in}}$ isthecut-inwindspeed.v_{rated}istheratedwindspeed.$v_{\text{cut-out}}$isthecut-outwindspeed.

Generator Model: the electrical power output from the wind turbine generator depends on the mechanical power captured from the wind and the generator's efficiency. It can be represented as:

$$P_{\text{gen}} = \eta_{\text{gen}} \cdot P_{\text{turbine}} \quad (13)$$

where η_{gen} is the generator efficiency.

Transmission and Distribution Losses: the power delivered to the grid is further reduced by losses in the transmission and distribution system:

$$P_{\text{grid}} = P_{\text{gen}} - P_{\text{loss}} \quad (14)$$

Differential equations are used to describe the mechanical and electrical dynamics involved in wind turbine reaction to changing wind conditions. Pitch, yaw, and torque control are examples of control strategies that maximize performance. Statistical distributions for wind speed at hub height are used in wind resource models. Turbulence and air density are examples of environmental factors that affect turbine performance. Real-world wind energy conversion system models grow complex and are frequently simulated using programs such as FAST. Key formulas and parts are needed to model a doubly fed induction generator (DFIG) in wind systems.

The stator equations for a DFIG are similar to those of a standard induction generator. The stator currents i_{as}, i_{bs}, i_{cs} are related to the stator voltages v_{as}, v_{bs}, v_{cs} and stator resistance R_s :

$$v_{as} = R_s i_{as} + L_s \frac{di_{as}}{dt} + p\lambda_m sri_{ar} \quad (15)$$

$$v_{bs} = R_s i_{bs} + L_s \frac{di_{bs}}{dt} + p\lambda_m sri_{br} \quad (16)$$

where

L_s is the stator self-inductance.

sis the slip frequency.

p is the number of pole pairs.

λ_m is the magnetizing current coefficient.

i_{ar}andi_{br} are the real and imaginary parts of the rotor current.

r is the rotor resistance.

The rotor equations describe the rotor currents i_{ar}, i_{br} and rotor voltages v_{ar}, v_{br} in terms of slip frequency, rotor resistance, and rotor inductance L_r:

$$v_{ar} = R_r i_{ar} + L_r \frac{di_{ar}}{dt} - p\lambda_m sri_{as} \quad (17)$$

$$v_{br} = R_r i_{br} + L_r \frac{di_{br}}{dt} - p\lambda_m s r i_{bs} \tag{18}$$

Torque Equation:

The electromagnetic torque T_{em} generated by the DFIG is related to the rotor currents and voltages:

$$T_{\text{em}} = \frac{3}{2} p\lambda_m \left(i_{ar} i_{bs} - i_{br} i_{as}\right) \tag{19}$$

Mechanical Equations:

The mechanical equations describe the rotational dynamics of the DFIG's shaft. The mechanical torque T_{m} applied to the shaft and the electromagnetic torque are related by the moment of inertia J and the angular acceleration ώ:

$$J\frac{\text{d}\omega}{\text{d}t} = T_{\text{m}} - T_{\text{em}} \tag{20}$$

DFIGs often incorporate control strategies to regulate various parameters. These strategies may include pitch control, active and reactive power control, and rotor-side converter control.

When connected to the grid, the DFIG's behavior is influenced by the grid voltage and frequency. Equations related to the grid-side converter are used to control the interaction between the DFIG and the grid.

These equations provide a foundation for modeling a Doubly Fed Induction Generator. To perform simulations and analyzes, software tools like MATLAB/Simulink, and specialized DFIG simulation packages can be used to create and study dynamic models of DFIG-based wind energy systems.

Static Var Compensator (SVC)

In order to maintain a constant voltage level on a bus, a Static VAR Compensator (SVC) is a device that effectively controls capacitive or inductive currents in an electrical power system. The inductance can be continuously changed from zero to its maximum value. These components define the operational range of the SVC and enable it to create or absorb the required reactive power as necessary.

The simplified diagram of the SVC and its control model is depicted in Fig. 5.

The core configuration of the TCR encompasses a fixed reactor with an inductance denoted as 'L', along with two bidirectional thyristor valves connected in series. These valves serve for conduction and blocking modes and are regulated using a firing angle indicated byα.

The instantaneous phase voltage '$v(t)$' in the Static Var Compensator (SVC) equivalent circuit, as shown in Fig. 6a, can be represented by the following equation:

$$v(t) = \sqrt{v_{dc}^2 + v_{ac}^2 \cdot \sin(\omega t - \phi)} \tag{21}$$

In this equation, v_{dc} represents the DC voltage component, v_{ac} stands for the AC voltage component, ω is the angular frequency, t- denotes time, and ϕ represents the phase angle. For the calculation of current in the equivalent circuit of the SVC as presented in Fig. 6b, The instantaneous current is calculated as:

$$I_L(\omega t) = \frac{\sqrt{2V}}{X_L}(\sin(\omega t) - \sin(\alpha)) \tag{22}$$

The relationship $\sigma = \phi - 2\alpha$ suggests that the conduction angle σ can be determined by subtracting twice the firing angle 2α from the phase angle ϕ. This equation is useful for calculating the portion of each AC cycle during which the thyristor conducts, based on when it is triggered to start conducting (the firing angle).

The control voltage at the SVC bus is denoted as the input, ΔV_{svc}. The susceptance value is determined by the firing angle

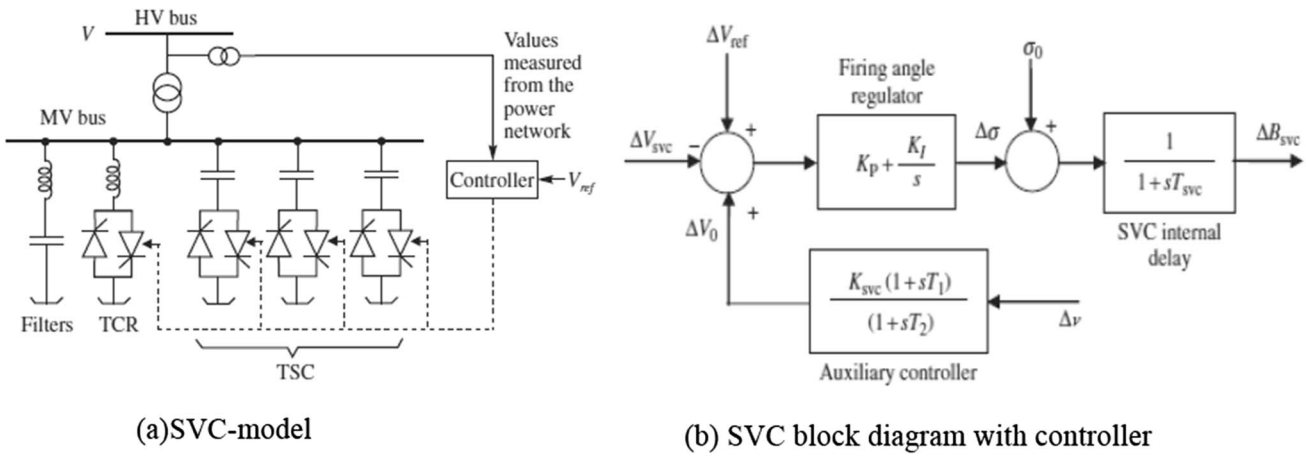

Fig. 5 Diagram of the SVC and control system

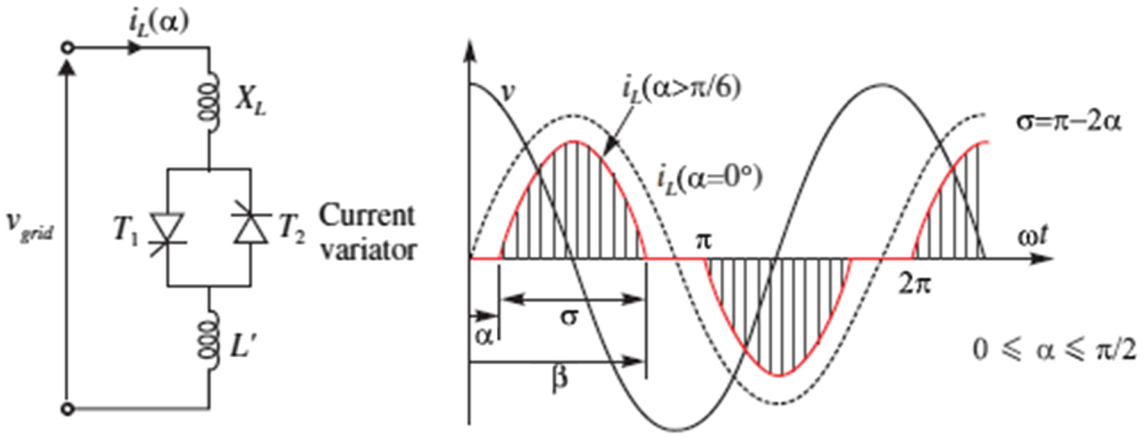

Fig. 6 Operation and analysis of SVC

and is regulated through a proportional-integral (PI) control loop with reference voltage V_{ref} for the SVC, as illustrated in Fig. 6b.

The linearized state-space representation is as follows:

$$\Delta\dot{V}_0 = -\frac{1}{T_2}\Delta V_0 + \frac{k_{\text{svc}}}{\omega_s}\left(\frac{1}{T_2}\right)\Delta\omega + \frac{k_{\text{svc}}}{\omega_s}\left(\frac{T_1}{T_2}\right)\Delta\omega$$

$$\Delta\dot{\alpha} = -k_1\Delta V_0 + k_1\Delta V_{\text{svc}} - k_1\Delta V_{\text{Ref}}$$

$$\Delta\dot{B_{\text{svc}}} = -\frac{1}{T_{\text{svc}}}\Delta\alpha - \frac{1}{T_{\text{svc}}}\Delta B_{\text{svc}} \tag{23}$$

Here, T_1, T_2, andT_{svc} denote lead, lag, and time delay constants, respectively, while k_{svc} represents the gain constant.

The linearized reactive power induced by the SVC at bus 'n' in the network is calculated using:

$$\Delta Q_n = \frac{\mathrm{d}Q_n}{\mathrm{d}\theta_n}\Delta\theta_n + \frac{\mathrm{d}Q_n}{\mathrm{d}V_n}\Delta V_n + \frac{\mathrm{d}Q_n}{\mathrm{d}\alpha}\Delta\alpha \tag{24}$$

Given that $Q_n = -B_{\text{svc}}V_n^2$, the equation is modified as:

$$Q_n = -B_{\text{svc}}V_n^2 \times \left[\,0 \;\; -2V_nB_{\text{svc}} \;\; 2V_n^2\left(1-\cos\tfrac{2\alpha}{X_L}\right)\right] \tag{25}$$

$$\begin{bmatrix}\Delta P_n\\ \Delta P_n\end{bmatrix} = \begin{bmatrix}0 & 0 & 0\\ 0 & -2V_nB_{\text{svc}} & 2V_n^2\left(1-\cos\tfrac{2\alpha}{X_L}\right)\end{bmatrix}\begin{bmatrix}\Delta\theta_n\\ \Delta V_n\\ \Delta\alpha\end{bmatrix} \tag{26}$$

Analysis of Faults with Symmetrical Components

A methodical approach to fault-based network analysis of power systems, with a particular emphasis on fault types including Single-Line-to-Ground (SLG), Line-to-Line-Ground (DLG), and Three-Phase-Ground (3Phase) faults. The system must be changed from the phase frame (a–b–c) to the sequence frame (1–2–0) and the sequence network must be connected according to the type of fault. Here is a more thorough explanation of each step:

As an illustration, for a single-line-to-ground fault, the current in phase-a (Ia) can be calculated as follows:

$$I_a = \frac{3V_a}{Z_0 + Z_1 + Z_2 + 3Z_f} \tag{27}$$

The fault current in phase-b (Ib) of the line-to-line-ground fault is computed as follows:

$$I_b = -\frac{j\sqrt{3}V_a}{Z_1 + Z_2 + Z_f} \tag{28}$$

And in the three-phase-ground fault, the fault currents in all three phases are calculated as:

$$I_a = \frac{V_a}{Z_1 + Z_f} \tag{29}$$

$$I_b = a^2 I_a \tag{30}$$

$$I_c = aI_a \tag{31}$$

The suggested fault analysis approach enables the evaluation of various problem kinds and aids in comprehending how the power system behaves when it has defects. To ensure the stability and dependability of the electrical grid, effective protection strategies can be adopted by precisely evaluating the fault conditions [19].

Machine Learning for Enhancing Power System Network Protection

The proposed smart transmission system for power networks incorporates machine learning and IoT technologies to enhance power system efficiency, staff safety, and fault detection capabilities. The system utilizes physical sensors, cameras, and measuring devices to collect real-time data from the power system. This data includes measurements such as voltage, current, and fault-inception angle. IoT technologies are employed to ensure efficient data collection and monitoring. The following sequence of task to be considered:

Data Collection and Processing

Collecting reliable and high-quality data is indeed crucial for training machine learning models effectively. The accuracy and performance of the model heavily depend on the quality of the data it receives. Here's a breakdown of the data collection process described in your statement:

The initial data is collected from the data center. This could include historical data, real-time measurements, or other relevant information from the power network. IoT devices, such as sensors and GPS satellites, are employed to gather data from various sources within the power network. These devices provide measurements, location information, and other relevant data. The collected data is sent to an expert data center, where it undergoes further processing and analysis. Simulation models and input data are used to initialize the wide area network data. This may involve setting up simulated scenarios or injecting specific data patterns into the network for testing and analysis. Machine code is employed to process and analyze the network data, extracting relevant features and patterns. The data collection and processing illustrated from Fig. 7.

Input Data Compilation and Visualization

Data from various sensors and monitoring devices installed throughout the transmission system are collected. This data may include voltage, current, frequency, phase angle, and other relevant parameters. The collected data is pre-processed to clean and normalize it. Data pre-processing techniques are used to handle missing values, remove noise, and prepare the data for further analysis. Relevant features are extracted from the data to represent specific patterns and characteristics of normal and fault conditions. Figure 8 illustrates the power system network in both healthy and faulty conditions, which can be seen in the example below.

Feature Extraction

A crucial phase in machine learning is feature extraction, which involves converting unprocessed data into a format that can be used to train models. To improve the model's predictive ability, pertinent data is condensed using methods like feature selection and dimensionality reduction. Improving model performance and generalization on untested data requires this procedure. The feature is extracted from training data which is from machine learning algorithm as shown in Fig. 9.

Model Selection and Training

Various machine learning algorithms, such as support vector machines (SVM), decision trees, random forests, or deep neural networks, can be employed. The selected

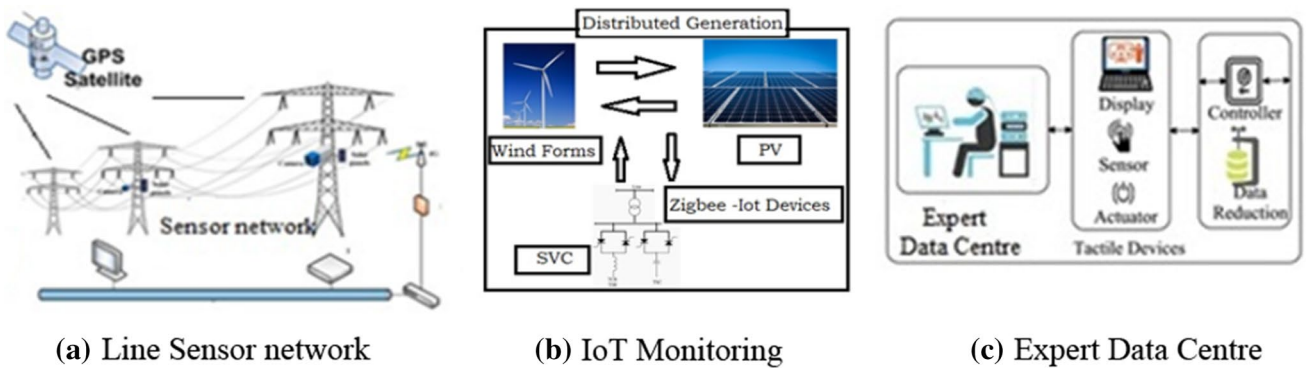

Fig. 7 Data collection and processing

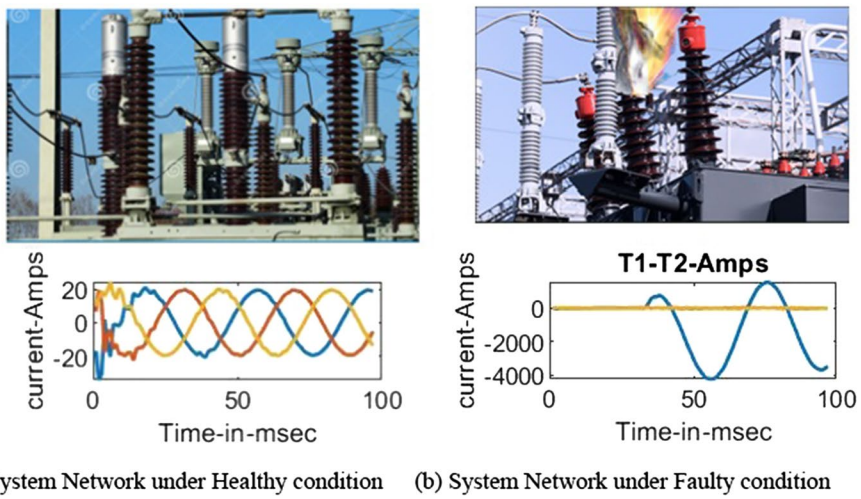

(a) System Network under Healthy condition (b) System Network under Faulty condition

Fig. 8 Visualization of network under healthy and fault condition

```
iaZ4=[];ibZ4=[];icZ4=[];iaZ44=[];ibZ44=[];icZ44=[];
iaZ444 = iaZ4-iaZ44;ibZ444 = ibZ4-ibZ44; icZ444 = icZ4-icZ44;
[CiaZ4,LiaZ4] = wavedec(iaZ4,1,'bior 1.5');
[CibZ4,LibZ4] = wavedec(ibZ4,1,'bior 1.5');
[CicZ4,LicZ4] = wavedec(icZ4,1,'bior 1.5');
[CiaZ44,LiaZ44] = wavedec(iaZ44,1,'bior 1.5');
[CibZ44,LibZ44] = wavedec(ibZ44,1,'bior 1.5');
[CicZ44,LicZ44] = wavedec(icZ44,1,'bior 1.5');

CD4_iaZ4 = detcoef(CiaZ4,LiaZ4,1);
CD4_ibZ4 = detcoef(CibZ4,LibZ4,1);
CD4_icZ4 = detcoef(CicZ4,LicZ4,1);
CD4_iaZ44 = detcoef(CiaZ44,LiaZ44,1);
CD4_ibZ44 = detcoef(CibZ44,LibZ44,1);
CD4_icZ44 = detcoef(CicZ44,LicZ44,1);

  Zone4_iaZ = (CD4_iaZ4-CD4_iaZ44);
  Zone4_ibZ = (CD4_ibZ4-CD4_ibZ44);
  Zone4_icZ = (CD4_icZ4-CD4_icZ44);
```

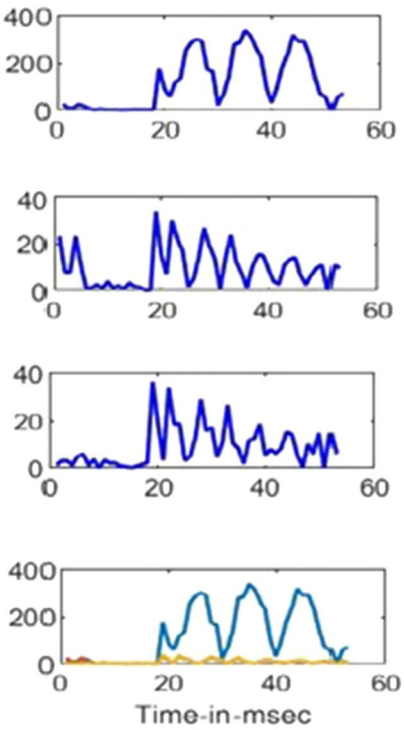

Fig. 9 Data collection and feature extraction through code implementation

model is trained using the training data, and it learns to recognize patterns associated with different fault conditions. The trained machine learning model analyzes real-time data from the transmission system and detects abnormal patterns that indicate the presence of faults. The model can classify the type of fault based on the patterns it has learned during training.

This helps in understanding the nature of the fault and aids in deciding the appropriate response. In some cases, additional sensors are used at different locations in the transmission system to enable the model to localize the fault accurately.

E. prediction of Result

The protection method can incorporate the machine learning model to continually and in real-time monitor the transmission system. The protection strategy can initiate automated procedures to isolate a malfunction and resume normal operation when one is discovered. The prediction of proposed

results are disseminated in Fig. 10 Additionally, the research encompasses an evaluation of network faults through positive, negative, and zero sequence components, which undergo mathematical analysis. The overarching goal of the research is to cultivate an intelligent transmission system that harnesses machine learning and IoT (Internet of Things) technologies to bolster power system protection, fault detection, and fault discrimination capabilities. The fusion of wavelet analysis [20], Support Vector Machine (SVM), and Artificial Neural Networks (ANN) enables effective and precise fault diagnosis and prediction, ultimately enhancing the reliability and performance of the power network [21–23].

Implementation Process: Case Study

The proposed scheme's combination of discrete wavelet transform and artificial neural networks holds great promise for enhancing fault detection and classification in transmission line protection. The use of wavelet analysis allows for a detailed examination of current samples, enabling the identification of specific fault patterns. By comparing wavelet detailed coefficients with other indices, faults can be efficiently detected and categorized. The fault detection algorithm, Polyfit analysis method tuning the test data to implement machine learning approach effectively. Overall, the proposed scheme's integration of wavelet analysis and artificial neural networks offers a promising approach to advance transmission system protection is presented in this research. By effectively detecting and locating faults, the scheme can significantly contribute to enhancing the overall reliability and resilience of power transmission networks.

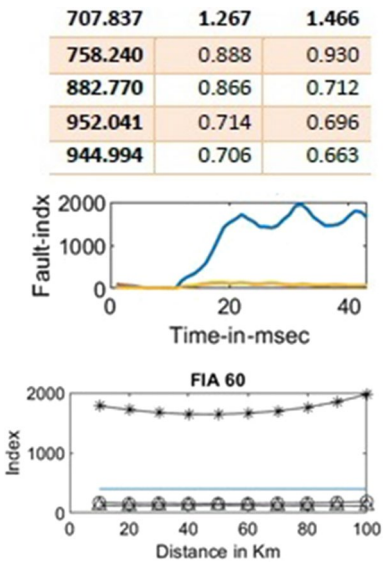

Fig. 10 Prediction of results

Addressing the challenges and fine-tuning the algorithms will be crucial to achieve optimal performance and ensure successful implementation in real world power systems.

In the realm of electrical protection techniques, supervised learning algorithms play a pivotal role, particularly through the utilization of Artificial Neural Networks (ANN) and Support Vector Machines (SVM), to conduct fault analysis and classification. To enhance the efficiency of fault detection and discrimination, the Integrated Moving Window Average Technique is harnessed. In the pursuit of uncovering concealed data patterns, unsupervised learning methods come into play. Meanwhile, the formulation of load balancing forecasts and fault detection within electrical system protection are two areas.

Where semi-supervised learning approaches are put to use. Wavelet analysis, specifically Bior1.5 mother wavelets, is utilized for analyzing steady-state and transient signals in fault discrimination and detection. Wavelet coefficients extracted from current waveform are used to train the ANN after calibrating Polyfit() function implementation, encoding the distance from the source to the fault based on wavelet indices. Multi-resolution analysis (MRA) of short-term current waveform is performed for micro-grid protection, facilitating fault detection. The sequence of machine learning process is discussed through Fig. 11.

Test System

These specifications provide an overview of the power system configuration, including the sources, transformers, line sections, and line parameters as shown in Fig. 12. It forms the basis for further analysis and modeling of the power system.

Based on the provided specifications, here are the details of the power system configuration:

Utility Grid: Terminal T1 and T2 with Power Rating: 500.

MVA/25 kV Connected through Transformer: 100 MVA, 25 kV/230 kV.

PV Source: Terminal T3 and T4 with Power Rating: 100 MVA/ 25 kV Connected through Transformer: 100 MVA, 25 kV/230 kV.

Wind Farm: Terminal T5: Wind Farm with Power Rating: 100 MVA/25 kV Connected through Transformer: 100 MVA, 25 kV/230 kV.

SVC: Connected in the middle of Zone-4 with Rating: 300 MVAR.

Area-I Specifications: Zone-1,Zone-2 and Zone-3 having distances of 25 km,10 km and 110 km.

Area-II Specifications: Zone-4,Zone-5 and Zone-6 having distances of 25 km,10 km and 110 km.

Line Parameters:

Resistance per Unit Length $R = 0.1153\ \Omega/\text{km}$; Zero-Sequence Resistance $R_0 = 0.4131\ \Omega/\text{km}$

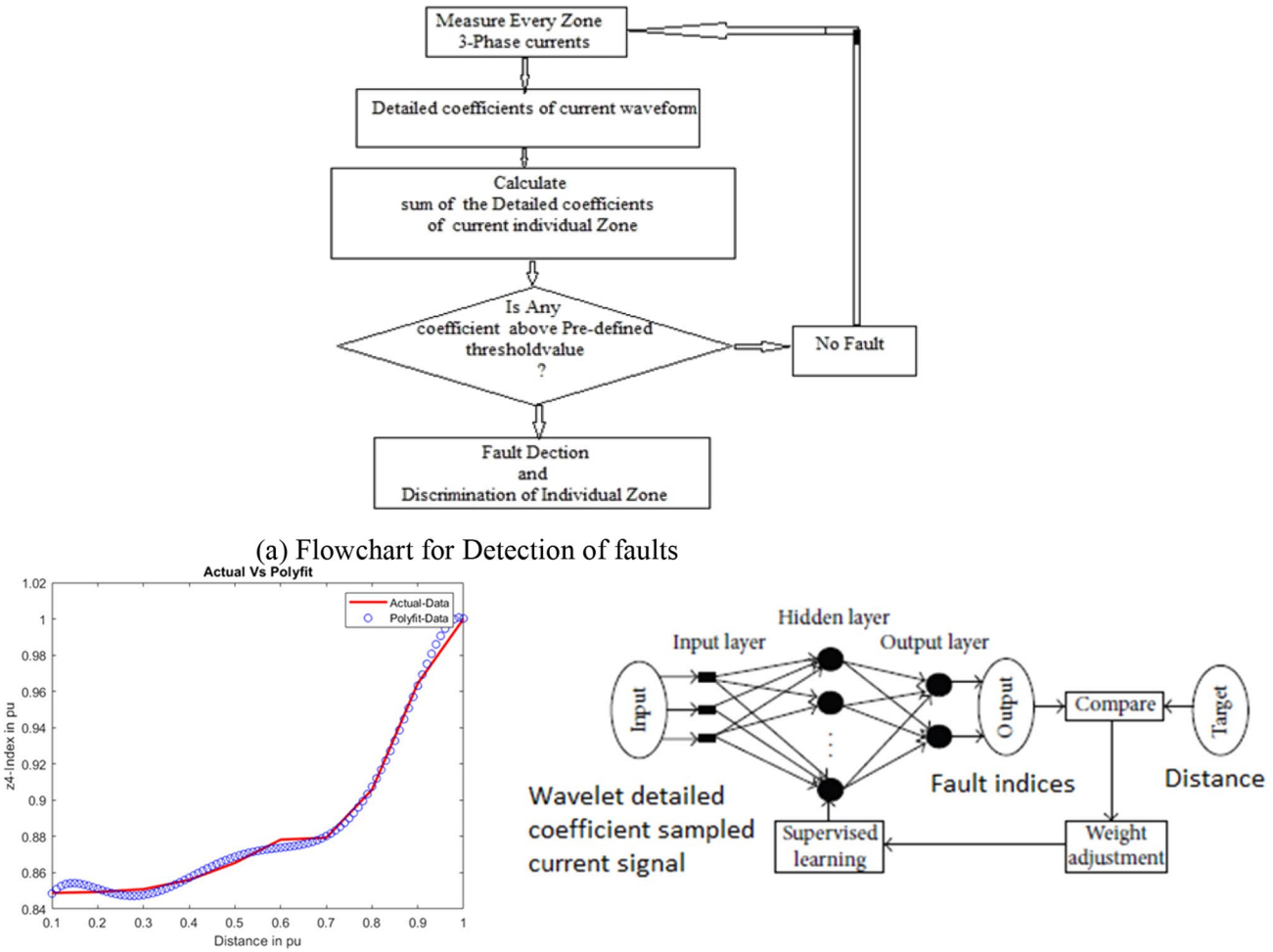

Fig. 11 Machine learning approach Implementation

Inductance per Unit Length $L = 1.053$ mH/km; Zero-Sequence Inductance $L_0 = 3.324$ mH/km

Capacitance per Unit Length $C = 11.33$nF/km; Zero-Sequence Capacitance $C_0 = 33.99$ nF/km

These values represent the key parameters used in modeling and analyzing power transmission lines in a power system.

Result Analysis

The proposed research work focuses on fault categorization, fault detection at particular fault inception angles (FIA), distances, and the effects of the Static Var Compensator (SVC). There are different types faults that are taken into consideration, such as single-phase to ground (1ϕG), two phase to ground (2ϕG), and three-phase to ground (3ϕG) faults.

The primary study cases encompass fault classification, varying faults at specific fault inception angles and distances. Detailed coefficients for each zone are calibrated to locate faults within that zone. Elevated index values, compared to the rest, indicate SLG, DLG, or TLG faults. The research further encompasses fault analysis at varying distances, with and without the presence of a compensated solar-PV connected system.

Phase analysis and fault identification are crucial aspects of power system management. Faults are accurately pinpointed by comparing 3-phase current index values with a threshold. When index values of faulty phases exceed the threshold while others remain below, the fault is located within those phases. Figure 13 illustrates fault identification using phase analysis based on current signals.

When doing Fault Analysis calibration, the impact of SVC (Static Var Compensator) compensation is taken into account when calculating the index at various distances during fault occurrences. In addition, the suggested methodology shows a decrease in quantum time when compared to conventional techniques. Figures 13, 14, 15 compare

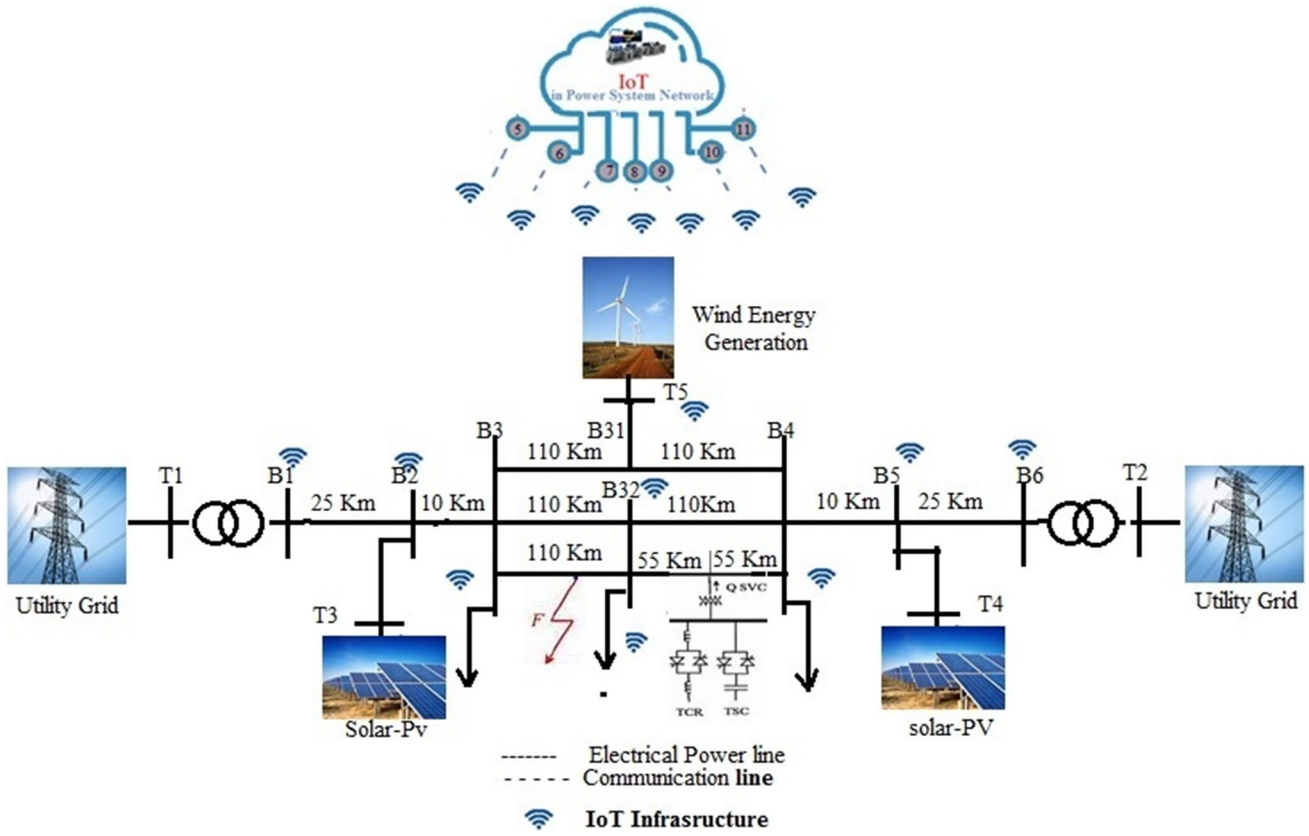

Fig. 12 Proposed wide-area power monitoring system

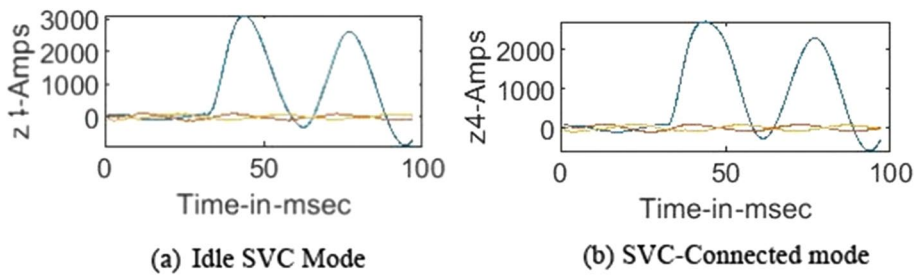

Fig. 13 current based fault identification

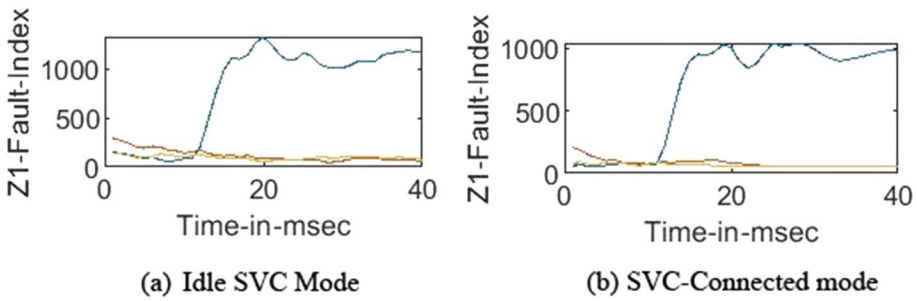

Fig. 14 Index based fault identification

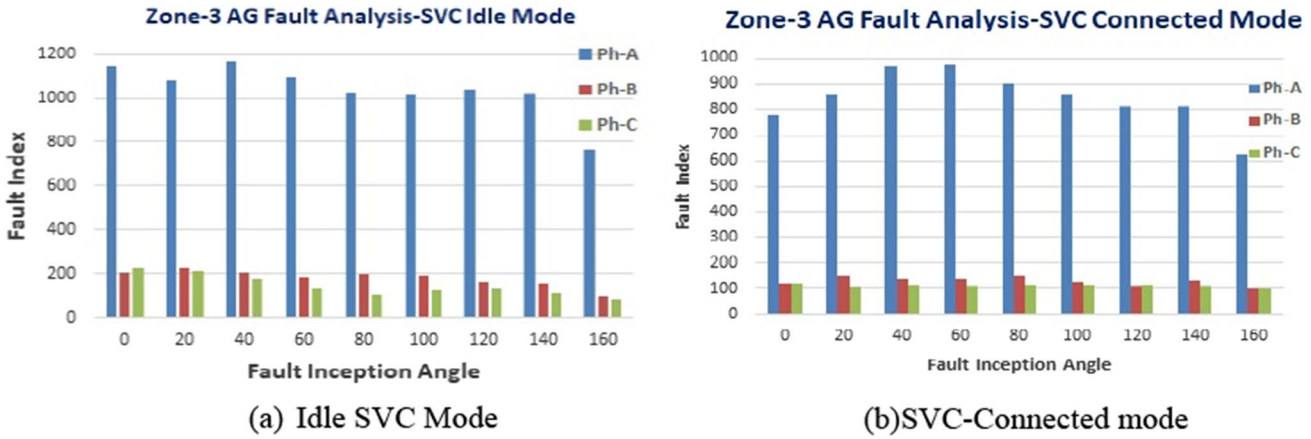

Fig. 15 Performance analysis of SVC under fault condition

different faults, distances, and fault initiation angles to demonstrate the effect of SVC.

The research focuses on fault classification, pinpointing fault inception angles and distances, and evaluating the role of SVC. The results underscore the efficacy of employing wavelet-based methodologies, particularly the sum-of-detailed coefficients technique, for accelerated fault identification. The investigation highlights the influence of SVC on fault severity, showcasing the proposed algorithm's ability to outperform considering current signal analysis (Fig. 13), fault identification demands a time quantum exceeding 40 ms, while the sum-of-detailed coefficients analysis (Fig. 14) accomplishes fault identification in less than 15 ms. This underlines the superiority of the proposed method compared to conventional techniques. Precise fault identification is achieved by scrutinizing 3-phase current index values against a predefined threshold. Instances where faulty phase index values surpass the threshold indicate that the respective phases are affected, while the remaining phases remain healthy (as illustrated in Fig. 14).

SVC compensation helps mitigate fault severity, potentially affecting relay operation based on predefined settings. Additionally, the research showcases a reduction in time quantum compared to traditional methods through the proposed algorithm. Figures 13, 14, 15, 16 highlight the impact of SVC by comparing various faults, distances, and fault inception angles.

The study primarily focuses on fault classification, pinpointing fault inception angles and distances, and evaluating the role of SVC. The efficacy of wavelet-based methodologies, particularly the sum-of-detailed coefficients technique, for accelerated fault identification is emphasized. The investigation underscores the superiority of the proposed method over conventional techniques in terms of time efficiency.

The research further encompasses fault analysis at varying distances, demonstrating the impact of SVC compensation on fault severity reduction. The study also acknowledges faults in discrete zones through the utilization of sum-of-the-detailed coefficients of the current signal. The recommended report stresses the method's ability to reduce time quantum, from around 0.40–0.15 s, compared to traditional methods. Finally, the impact of SVC is observed by comparing various faults, distances, and fault inception angles, as depicted in Figs. 15 and 16.

Fault analysis results with and without a compensated solar- PV linked system are shown in Table 1. It shows how to determine the type of fault independent of the fault's location or angle of initiation. Relay functioning based on preset

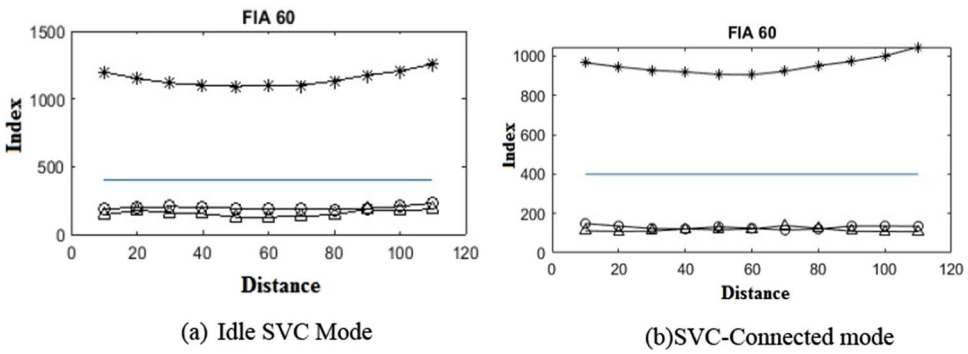

Fig. 16 Analysis of SVC performance under various fault inception angles

Table 1 Comparative Fault analysis with and without SVC Integrated system through Fault Indices at Zone-3

	PV-WIND-Integrated System						SVC-PV-WIND- Integrated System					
	0	15	30	60	75	90	0	15	30	60	75	90
	Phase-A Current FIA in degrees						*Phase-A Current FIA in degrees*					
10	1263.6	1259.0	1300.7	1231.7	1188.4	1148.1	938.33	1110.1	1116.6	1092.7	985.94	973.07
20	1174.8	1121.9	1222.6	1179.5	1132.7	1104.2	865.15	986.63	1069.6	1037.6	945.79	918.55
30	1192.6	1107.5	1194.8	1137.3	1075.0	1059.2	824.03	906.23	1001.7	1000.5	919.41	880.93
40	1149.7	1078.9	1167.8	1095.4	1024.9	1012.1	779.41	855.57	969.98	972.24	904.11	856.05
50	1180.9	1078.6	1162.5	1074.5	993.5	986.5	795.74	834.04	955.27	952.47	889.88	842.62
60	1179.3	1059.3	1141.4	1046.2	964.3	964.7	796.50	810.27	934.32	924.98	868.09	825.81
70	1155.9	1035.8	1127.0	1035.4	960.2	966.4	785.73	791.15	921.57	906.97	857.42	820.91
80	1129.3	1023.3	1126.7	1043.9	974.0	980.5	779.41	790.66	921.11	908.27	859.83	823.40
90	1117.1	1031.8	1127.6	1065.5	999.7	1007.6	785.58	810.38	925.37	919.84	864.07	824.51
100	1148.1	1054.7	1140.4	1086.3	1027.5	1037.6	799.41	833.61	933.33	928.40	868.60	827.99
	Phase-B Current FIA in degrees						*Phase-B Current FIA in degrees*					
10	251.47	266.23	251.09	207.06	191.61	168.17	111.66	126.73	121.65	116.65	134.18	116.06
20	249.71	260.97	245.71	221.97	201.70	178.71	117.20	128.09	135.27	132.71	141.26	122.44
30	196.44	230.72	207.17	186.18	197.01	177.83	130.58	140.74	128.72	135.85	146.87	122.52
40	205.84	221.30	204.92	184.54	197.06	189.61	122.86	149.35	138.46	136.12	147.05	127.04
50	178.93	210.87	192.08	182.33	185.20	187.74	130.13	130.07	114.30	121.08	139.77	122.35
60	156.77	187.11	180.24	176.14	176.30	172.10	110.34	116.36	101.01	114.36	135.27	114.23
70	141.39	180.60	175.20	169.46	180.33	172.77	96.66	115.76	101.10	123.01	149.02	121.84
80	161.02	193.82	175.89	166.10	186.37	175.80	92.28	119.63	109.02	131.04	153.84	122.99
90	213.04	224.55	194.18	175.13	190.98	178.45	108.04	133.08	110.24	120.91	143.28	120.58
100	219.25	243.50	200.52	195.85	205.81	188.17	115.68	132.68	113.01	123.94	137.70	118.98
	Phase-C Current FIA in degrees						*Phase-C Current FIA in degrees*					
10	276.56	244.88	259.00	187.67	144.47	178.72	133.87	118.59	131.33	123.66	124.83	120.92
20	245.75	218.91	206.13	159.48	126.31	152.43	154.33	126.75	117.52	108.23	118.13	117.03
30	243.32	235.01	218.11	147.76	120.23	143.79	160.65	123.91	125.15	107.15	113.18	120.70
40	227.71	212.22	180.30	130.17	102.41	127.16	119.10	103.55	115.71	108.29	113.99	118.59
50	252.25	233.84	190.77	146.53	112.41	134.69	178.18	138.41	140.80	124.05	120.29	122.39
60	259.85	234.72	205.23	173.11	129.47	148.74	214.23	161.73	172.04	141.25	127.39	129.85
70	241.85	216.19	186.36	148.84	116.86	146.05	194.69	152.50	160.97	123.11	118.90	118.99
80	214.70	200.08	162.84	127.78	107.50	139.69	174.61	144.88	149.18	117.66	118.68	117.13
90	201.12	198.87	150.59	129.66	104.82	129.19	161.57	142.06	140.21	121.95	119.20	118.17
100	213.17	218.14	158.84	146.57	124.76	150.83	182.30	147.92	130.0	110.20	113.48	115.33

Table 2 Error calibration using Actual Distance and ANN Calculated Distance at Zones 3 and 4

	Zone3: Fault type						Zone4: Fault type					
AD	CD	E	CD	E	CD	E	CD	E	CD	E	CD	E
20	20.04	−0.04	19.00	0.90	19.38	0.55	18.62	1.25	20.07	−0.06	19.78	0.20
30	30.55	−0.50	29.42	0.52	29.81	0.17	31.20	−1.09	30.11	−0.10	31.05	−0.95
40	40.11	−0.10	42.47	−2.24	43.02	−2.74	41.63	−1.48	43.78	−3.43	39.13	0.79
50	50.44	−0.40	51.40	−1.27	49.78	0.19	48.69	1.19	48.47	1.39	50.56	−0.50
60	59.01	0.89	61.52	−1.38	62.64	−2.40	63.49	−3.17	59.01	0.90	58.43	1.42
70	72.13	−1.93	69.25	0.67	69.02	0.88	66.63	3.06	69.35	0.59	70.39	−0.35
80	79.62	0.34	79.25	0.68	80.43	−0.39	80.78	−0.70	82.14	−1.94	79.54	0.41
90	89.39	0.55	91.53	1.38	91.86	−1.69	89.79	0.19	88.44	1.41	92.55	−2.31
100	99.68	0.28	99.65	0.31	100	−0.03	99.43	0.51	98.43	1.42	103.14	−2.85

AD actual distance, *CD-ANN* calculated distance, E-% Error

settings may be impacted by the use of SVC compensation, which helps to mitigate fault severity. Table 2 presents the % error analysis utilizing both real and ANN calibrated distance at different fault locations. The research shows that the actual distance varies very little between fault locations.

Conclusion

The incorporation of reactive power compensation devices and renewable energy sources, in conjunction with methodical maintenance protocols, is vital in guaranteeing the continuous distribution of electrical power across a country's grid. Furthermore, in order to reduce disturbances caused by both balanced and unbalanced electrical problems, a responsive security system is necessary. This work uses mathematical and electrical principles to investigate transitory signals through wavelet and machine learning techniques, providing important new insights into power network issues.

However, demand variations, the unpredictability of renewable energy supply, and the complexity of the grid, which is made worse by unidentified grid models, make it difficult to deploy reactive power devices and renewable energy sources. supervised and unsupervised machine learning techniques are used in this research to address these issues and progress power system analysis.

The suggested algorithm shows effectiveness in identifying and differentiating fault behavior in PV-Wind integrated power system networks, with or without Static Var compensators, by employing a wavelet-based machine learning technique. The findings show that the algorithm works better than conventional methods, providing a viable path for improving power transmission systems' dependability and efficiency in the face of changing energy environments.

Funding No funding was received.

Declarations

Conflict of interest The authors have not disclosed any competing interests.

References

1. S.R.M. Rahmatallah Poudineh, D. Peng, Electricity networks: Technology, future role and economic incentives for innovation. Oxford Ins. Energy Stud. EL. **7**, 5–14 (2017)
2. J. de Jesús, J. Serna, J.M. López-Lezama, Calculation of distance protection settings in mutually coupled transmission lines: A comparative analysis. Energies **12**(7), 1290 (2019). https://doi.org/10.3390/en12071290
3. G. Kolumbán, M.P. Kennedy, L.O. Chua, The role of synchronization in digital communications using chaos. i. fundamentals of digital communications. IEEE Trans. Circuits Syst. I Fundam. Theory Appl. **44**(10), 927–936 (1997)
4. J.X.Y. Wang, T. Bian, C. Wen, Global synchronization of complex dynamical networks through digital communication with limited data rate. IEEE Trans. Neur. Netw. Learn. Syst. **26–10**, 2487–2499 (2015)
5. E. Sortomme, G.J. Mapes, S.S. Venkata, Microgrid fault location: Challenges and solutions. Fault Anal. Protec. Microgrid **76**, 1–6 (2008). https://doi.org/10.1109/NAPS.2008.5307360
6. S.S. Gururajapathy, H. Mokhlis, H.A. Illias, Fault location and detection techniques in power distribution systems with distributed generation: a review. Renew. Sust. Energy Rev. **74**, 949–958 (2017). https://doi.org/10.1016/j.rser.2017.03.021
7. A. Ghorbani, M. Khederzadeh, Impact of svc on the protection of transmission lines. Int. J. Electr. Power Energy Syst. **42**, 702–709 (2012). https://doi.org/10.1016/j.ijepes.2012.04.029
8. S. Francois, J. Datta, Svc protection and control basics (for entergy's porter svc with external capacitor bank switching). In: 58th Annual Conference for Protective Relay Engineers, pp 86–95 (2005)
9. N.K.M.A.R.M.R. Bishal, S. Ahmed, M.A.A. Hysam, Ann based fault detection classification in power system transmission line. In: International Conference on Science Contemporary Technologies (ICSCT), **70**, pp 1–4 (2021). https://doi.org/10.1109/ICSCT53883.2021.9642410
10. Y. Aslan, An alternative approach to fault location on power distribution feeders with embedded remote-end power generation using artificial neural networks. Electr. Eng. **94**, 125–134 (2012)
11. H. Yang, X. Liu, D. Zhang, T. Chen, C. Li, W. Huang, Y. Hanyu, L. Xubin, Machine learning for power system protection and control. Elect. J. **34**(1), 106881 (2021). https://doi.org/10.1016/j.tej.2020.106881
12. H. Bashiri Mosavi, Hosseini, A learning framework for size and type independent transient stability prediction of power system using twin convolutional support vector machine. IEEE Access **6**, 69937–69947 (2018)
13. U.D.A.I.T.F.F.R. Gomez, A.D. Rajapakse, Support vector machine- based algorithm for post-fault transient stability status prediction using synchronized measurements. IEEE Trans. Power Syst. **26**, 1474–1483 (2011)
14. B. Edward, Application of wavelet technique for fault classification in transmission systems. Procedia Comput. Sci. **92**, 78–83 (2016)
15. H. Athabadi, Impact of high-voltage power transmission lines on photo- voltaic power production. Sol. Energy **163**, 78–83 (2018)
16. Z. Mohamed, A. Eltawil, Mppt techniques for photovoltaic applications. Renew. Sust. Energy Rev. **25**, 793–813 (2013)
17. Z.M. Haidar, H. Chible, D.D. Caviglia, Dan optimized ac/dc buck boost converter for wind energy harvesting application. IEEE Ind. Comm. Power Syst. Europe (EEEIC/ICPS Europe) (2019). https://doi.org/10.1109/EEEIC.2019.8783648
18. M.R.L.A. Kumar, Modeling and simulation of a DFIG based wind energy system. Adv. Smart Grid Technol. **687**, 31–49 (2020)
19. A.T.R.S. Goli, Fuzzy-wavelet based double line transmission system protection scheme in the presence of svc. J. Inst. Eng. India Ser. B **96**, 131–140 (2015). https://doi.org/10.1007/s40031-014-0130-z
20. W. Hanyu Yang, X. Liu, Machine learning for power system protection and control. Elect. J. (2021). https://doi.org/10.1016/j.tej.2020.106881
21. R. Morello, C. De Capua, S.C. Mukhopadhyay, A smart power meter to monitor energy flow in smart grids: The role of advanced sensing and IOT in the electric grid of the future. IEEE Sens. J. **17**, 7828–7837 (2017)
22. S.L.S. Chandra Shekar, G. Ravi Kumar, Renewable energy integrated multi-terminal transmission system using wavelet based

protection scheme. Int. J. Power Elect. Drive Syst. (IJPEDS) **10**, 995–1002 (2019)
23. J.A. Martin, Aguado, Wavelet-based ANN approach for transmission line protection. IEEE Trans. Power Delivery **18**, 1572–1574 (2003). https://doi.org/10.1109/TPWRD.2003.817523